Article:
Li, B, Wang, Z, Vivacqua, V et al. (7 more authors) (2020) Drop-interface electrocoalescence mode transition under a direct current electric field. Chemical Engineering Science, 213. ISSN 0009-2509

https://doi.org/10.1016/j.ces.2019.115360

Drop-interface electrocoalescence mode transition under a direct current electric field

Bin Li[a,b],Zhentao Wang[a], Vincenzino Vivacqua[b], Mojtaba Ghadiri[b], Junfeng Wang[a,*], Wei Zhang[a], Dongbao Wang[a], Hailong Liu[a], Zhiqian Sun[c], Zhenbo Wang[c]

[a] *School of Energy and Power Engineering, Jiangsu University, Zhenjiang 212013, China*

[b] School of Chemical and Process Engineering, University of Leeds, Leeds LS2 9JT, UK

[c] *State Key Laboratory of Heavy Oil, China University of Petroleum (East China), Qingdao 266580, China*

Abstract: The electrocoalescence of a water drop at the water/oil interface in the presence of externally direct current electric fields was numerically analyzed with the finite element method by solving the Navier-Stokes and charge conservation equations. The proprietary software Comsol Multiphysics was used for this purpose, and the interface motion was captured by the Level-Set method. Good agreement was obtained between numerical and experimental results in the literature. The effects of the electric field strength, droplet size, oil phase permittivity, surface tension, bulk viscosity, water phase conductivity, and drop-interface distance were systematically assessed. Three coalescence modes were obtained:

* *Corresponding author.*
E-mail address: wangjunfeng@ujs.edu.cn (J. Wang).

complete coalescence, including typical complete coalescence and complete coalescence with upheaval; partial coalescence, including typical partial coalescence and jet-like partial coalescence; and non-coalescence, including typical non-coalescence and breakup of bouncing-off droplet non-coalescence. The pressure gradients between the drop and the bridge rather than the sign of the pressure determined the coalescence. There is a critical non-dimensional drop-interface distance of electrocoalescence modes that has negligible dependence on the non-dimensional water phase conductivity. The ratio of the Weber Number (describing electric field effects) and the Ohnesorge Number (describing physical properties) was found to well describe the coalescence process. The outcome of this work is potentially useful for optimizing the design of compact and efficient oil-water separators.

Keywords: Electrocoalescence; Drop-interface coalescence; Level-Set method; Interface; Electrohydrodynamics

1. Introduction

Crude oil, extracted from reservoirs, contains a significant amount of saline water in a dispersed phase accompanied by resins, asphaltenes, and paraffins, which stabilize the dispersion because they act as surfactant (Mhatre et al., 2019; Mhatre et al., 2015). The amount of water also increases with the age of the well (Eow and Mojtaba, 2001). Moreover, some oil production methods, e.g. steam-assisted gravity drainage (SAGD), generate

a large amount of water, which has been as much as 90 wt% in recent years (Li et al., 2017a). As a consequence, stable water-in-oil (W/O) emulsions (Yu et al., 2018) are readily formed during the crude oil production stage, causing problems in the oil industry, such as equipment corrosion, catalyst poisoning, and extra transportation cost (Eow and Mojtaba, 2001; Mousavi et al., 2014; Taylor and design, 1996). Therefore, efficient methods to remove the water phase from the oil phase are highly desirable and will have significant financial benefits. Several techniques (Goto et al., 1989; Hirato et al., 1991; Li et al., 2017c; Mohammed et al., 1994; Mousavichoubeh et al., 2011b; Sun et al., 1999) have been applied to improve the separation efficiency. Electrostatic demulsification stands out among these methods because of its low operating costs and environmentally-friendly nature (Eow and Mojtaba, 2001; Luo et al., 2016; Mhatre et al., 2015). However, some researchers (Aryafar and Kavehpour, 2009, 2010; Aryafar and Kavehpour, 2007; Mousavi et al., 2014; Mousavichoubeh et al., 2011a; Mousavichoubeh et al., 2011b) reported that in an excessively high electric field, partial coalescence could occur, which has adverse effects on the separation efficiency of water droplets from the oil. Moreover, most of the commercially available electrocoalescers are large and bulky, which is due to lack of underlying fundamental knowledge of the governing effects of electric fields on drop-drop coalescence and drop-interface coalescence in the oil phase (Eow et al., 2002; Eow and Mojtaba, 2001; Mhatre et al., 2015; Wang et al., 2018).

In the absence of an electric field, three stages are included during the coalescence process, i.e. drop-drop approach (in drop-drop coalescence)

or drop-interface approach (in drop-interface coalescence); film thinning, which is the overall controlling step and is affected by the capillary pressure and disjoining pressure (Rommel et al., 1992); and film rupture and coalescence (Holto et al., 2009; Luo et al., 2018; Sun et al., 1999). Applying an electric field, the approach process is accelerated and the film thinning process is significantly enhanced , which substantially improves the coalescence and separation efficiency (Li et al., 2017b; Li et al., 2016; Vivacqua et al., 2015). However, electrocoalescence suffers from break-up and formation of secondary droplets, which undermine the separation process of the water phase from the oil phase. Aryafar and Kavehpour (Aryafar and Kavehpour, 2007) reported that at a sufficiently low Ohnesorge number, secondary droplets can sometimes form in the absence of electric field. The application of an external electric fields, however, results in a large interface perturbation and large secondary droplet formation. In addition, strong electric fields can result in the formation of a secondary jet rather than a droplet. At intermediate field strengths, semi-stable jets which protrude from the droplet apex are more likely to form. At sufficiently high strengths, the jets form much earlier and they exhibit electrospraying and electrospinning behavior (Aryafar and Kavehpour, 2010). Moreover, in Aryafar and Kavehpour's pioneering work (Aryafar and Kavehpour, 2009), by appropriately scaling the electric field, distinct regions of behavior were defined in which electrically induced partial coalescence occurred within a viscous environment. In addition, they reported that under sufficiently high direct current electric fields, droplet size and field strength determine either jet formation or Taylor cone formation during the partial coalescence on the planar interface.

Ristenpart et al. (Ristenpart et al., 2009) reported that oppositely charged drops coalesced at low field strength while they repelled one another in a high electric field. Mousavichoubeh et al. (Mousavichoubeh et al., 2011a) reported that the pumping process (due to the surface tension) and necking process (due to the electric field) operated simultaneously during the drop-interface coalescence. Whether a secondary droplet is formed depends on which process is dominant, i.e. pumping resulting in complete coalescence and necking resulting in partial coalescence. Hamlin et al. (Hamlin et al., 2012) reported the existence of a critical ionic conductivity below which oppositely charged drops only partially coalesced. Wang et al. (Wang et al., 2014) reported that a crown profile of drop fission always appear on the top surface of negatively charged drops after two charged drops contact and bounce off. They argued that the Coulomb fission might be caused by Rayleigh instability, and that the different mobility of positive and negative ions is the underlying mechanism which accounts for the invariable occurrence of break-up on the negative side of charged drops. Though researchers have done many experimental investigations on partial electrocoalescence, most of them focused on the effects of external parameters, e.g. electric and physical parameters, and the effects of internal dynamics of drops, such as capillary pressure field distribution during the coalescence, was far from being determined.

In order to optimize the design of electrocoalescers, it is highly beneficial to understand the internal dynamics that favor complete, partial, and non-coalescence. Charge transfer has been generally acknowledged to play important roles in the electrohydrodynamics of coalescence (Atten

and Aitken, 2010; Hamlin et al., 2012; Saranin and Physics, 2011; Vivacqua et al., 2016). However, Bird et al. (Bird et al., 2009) proposed an innovative theory that the pressure difference, which is affected by the contact angle between the drop and the liquid bridge dominates the flow direction. The dominant role of the electric field is to distort the drops before contact, while the subsequent dynamics predominantly depend on the capillarity. Moreover, Bartlett et al. (Bartlett et al., 2015) reported that the transition between coalescence and recoil is determined by the conical drop topology rather than charge effects. Helmensdorfer (Helmensdorfer and Topping, 2013) used the mean curvature flow theory to explain the non-coalescence of charged droplets, which indicates that the minimization of energy can, contrary to general belief, explain the coalescence phenomenon. Choi et al. (Choi et al., 2016) investigated the morphological characteristics of coalescing droplets and reported that the curvature of the liquid bridge determines the pressure difference. Therefore, the pressure difference is the driving force for the liquid bridge evolution (Luo et al., 2018; Ristenpart et al., 2009), however, few literatures have reported the impact mechanism (TEIGEN et al., 2006; Xin et al., 2017). From the above reports, it seems that the capillary pressure field distribution can have an important impact on the electrocoalescence, however, it has received scant attention in the literature, in part due to the difficulties to experimentally measure the field distribution during the fast coalescence process (within a millisecond) and the complexities involved in modeling a two-phase electrophoretic flow. Therefore, a mathematical description, which was established in the present study, is needed for an intense study of the impact of capillary pressure during

coalescence.

Numerical simulation is a rapid tool for the extrapolation of the above results to more general cases and to provide guidelines to determine the operating conditions under which the elctrocoalescence efficiency is enhanced. Droplet behaviors have been numerically investigated explicitly and implicitly with the droplet interface described by using interface tracking and interface capturing methods, respectively (Li et al., 2017c). In the former, discrete points are tracked on the interface surface, including the front tracking method and the boundary integral method (Collins et al., 2008). The implicit methods include the Level-Set, Volume of Fluid (VOF), and Phase-Field, which are well suited to calculate topological changes and widely used to model droplet motion, deformation, and coalescence (Shadloo et al., 2013). The Level-Set method (Sethian, 1999), which was adopted in the present study, can predict the effect of surface tension slightly more accurately, which is vital in reproducing pinching and formation of secondary droplets. Li et al. (Li et al., 2017c) investigated droplet deformation under pulsatile electric fields in the case of half-sinusoidal, square, and sawtooth waves by the Level-Set method, which showed good agreement with the experimental work. A few numerical attempts (Table 1) have been conducted to predict the occurrence of partial coalescence in the absence and presence of electric fields. Blanchette et al. (Blanchette and Bigioni, 2006) numerically studied the partial coalescence of liquid drops onto the surface of an identical liquid in air (while liquid surroundings were modelled in the present study), and reported that partial coalescence is a dynamically driven process that does not result

from the Rayleigh-Plateau instability. Yue et al. (Yue et al., 2006) conducted a computational study of drop-interface coalescence in Newtonian and viscoelastic fluids using the phase-field method and reported that partial coalescence proceeds in two stages: propagation of capillary waves along the drops and formation of a fluid column; and neck formation on the column and pinching-off of the secondary drop. However, they focused on the effects of viscoelasticity, which was also mainly studied by Blanchette et al. (Blanchette and Bigioni, 2009), in the process, but the underlying internal mechanism of partial coalescence was still unclear. In addition, in their work, no external electric field was applied, and the electrohydrodynamics of the two-phase electrophoretic flow in the partial coalescence was therefore not included. Teigen et al. (TEIGEN et al., 2006) modeled the coalescence process between a drop and an interface in an electric field, and reported that electric fields produce higher pressures inside the drop. However, the physics of charge relaxation was not considered, which has been included in the present work. Hongmiao et al. (Hongmiao et al., 2011) presented a new approach for numerical simulation of partial coalescence based on the coupling of liquid dielectrophoresis and two-phase flow theories. However, they mainly focused on the geometry of the high-voltage electrode, e.g. flat and patterned electrodes, rather than the internal dynamics. Karyappa et al. (Karyappa, 2014) conducted a detailed numerical and experimental analysis of droplet behaviors prior to breakup, while the occurrence of the progeny droplet was only experimentally investigated. Pillai et al. (Pillai et al., 2017) proposed an electrokinetic model to numerically investigate charge transfer dynamics during the electrocoalescence process of a microdrop and interface, while

ignoring the capillary pressure. Vivacqua et al. (Vivacqua et al., 2016) proposed a model of drop-interface electrocoalescence under a constant electric field by the Level-Set method, which showed good agreement with the experimental work by Mousavichoubeh et al. (Mousavichoubeh et al., 2011b). However, their work mainly focused on the accuracy improvement of the model by considering the effects of the mesh size, interface thickness, and re-initialization parameter, and paid no attention to the mechanism for mode transition of the coalescence process because of the lack of systematical analysis of key factors (which was conducted in the present work) that influence the process.

< Table 1 The conclusions of the numerical literatures and the novelty of the present work >

In the light of the above considerations, the overall picture related to the influence of internal dynamics of partial coalescence is fragmentary. It has recently been reported that charge transfer significantly influences the electrocoalescence, however, the present study attempted to provide another insight into the coalescence process from a viewpoint of capillary pressure, by using an approach for numerical simulation proposed in the previous work (Li et al., 2017c; Vivacqua et al., 2016). For this purpose, a finite element approach combined with the Level-Set method was used to analyze the process of drop-interface electrocoalescence. The present study mainly focused on the evolutions of the internal pressure field in

different electrocoalecence modes in order to determine the underlying internal mechanism of mode transition. In addition, in this study, new coalescence modes were obtained and the effects of electric (electric field strength), physical (surface tension, bulk phase viscosity and permittivity, dispersed phase conductivity, droplet size), and operating (initial drop-interface distance) parameters on the coalescence dynamics and modes were systemically assessed, and a scaling relation was developed for the normalized volume of secondary droplets as a function of the coupling effect of electric (accounting for the intensification of the necking process) and physical (accounting for the rate of pumping) parameters.

2. Model description

The proprietary software Comsol Multiphysics was used to conduct the simulations. The computational model used a 2-D axisymmetric domain schematically shown in Fig. 1(a). A close-up of the domain near the oil-water interface is given in Fig. 1(b) to show the quality of the mesh generated with h_{max}/D=0.03, where h_{max} is the maximum mesh element size and D is the droplet diameter. The boundary conditions used in the present study were as follows: the upper boundary was a direct current potential U, the bottom boundary was kept earthed, both the upper and the bottom boundaries were no-slip ones, while the right boundary had a slip condition ($\mathbf{u}\cdot\mathbf{n}$=0), which significantly reduced the simulation domain.

<Fig. 1 (a) Sketch of the simulation domain. (b) Close-up of the mesh for h_{max}/D=0.03.>

The Level-Set method was utilized to track the boundaries between the water and oil phase. The interface was obtained by solving the transport equation of the Level-Set function ϕ and described by ϕ=0.5 (Li et al., 2017c; Vivacqua et al., 2016). The evolution of the boundary is shown by Eq. (1) (Olsson and Kreiss, 2005).

$$\frac{\partial \phi}{\partial t} + \mathbf{u}\nabla\phi = \lambda\nabla\cdot(\xi\nabla\phi - \phi(1-\phi)\frac{\nabla\phi}{|\nabla\phi|}) \quad (1)$$

where $\mathbf{u}$ is fluid velocity, ϕ is a smooth step function (range of 0-1), λ is a re-initialization parameter to stabilize the solution, and ξ determines the interface thickness.

We followed the approach of Li and Vivacqua et al. (Li et al., 2017c; Vivacqua et al., 2016), coupling Eq. (1) with the Navier Stokes equations for the flow and Laplace equations for the electric field. The capillary and electric forces were also included in the Navier Stokes equations as follows.

$$\rho(\phi)\frac{\partial \mathbf{u}}{\partial t} + \rho(\phi)(\mathbf{u}\cdot\nabla)\mathbf{u} = -\nabla p + (\mu(\phi)(\nabla\mathbf{u} + \nabla\mathbf{u}^{T})) + \mathbf{F}_{\gamma} + \mathbf{F}_{E} \quad (2)$$

$$\nabla\cdot\mathbf{u} = 0 \quad (3)$$

$$\rho(\phi) = \rho_{\mathrm{w}} + (\rho_{\mathrm{o}} - \rho_{\mathrm{w}})\phi \quad (4)$$

$$\mu(\phi) = \mu_{\mathrm{w}} + (\mu_{\mathrm{o}} - \mu_{\mathrm{w}})\phi \quad (5)$$

where p is the fluid pressure, $\mathbf{F}_\gamma$ is the interfacial force, $\mathbf{F}_\mathbf{E}$ is the electric force, ρ_w is the density of water, ρ_o is the density of oil, and μ_w and μ_o are the viscosities of water and oil, respectively.

The interfacial tension force $\mathbf{F}_\gamma$ is calculated by:

$$\mathbf{F}_\gamma = \nabla \cdot (\gamma(\mathbf{I} - (\mathbf{n}\mathbf{n}^{\mathrm{T}}))\delta) \quad (6)$$

where γ is the surface tension coefficient, $\mathbf{I}$ is the identity matrix, $\mathbf{n}$ is the interface normal, and δ is a smooth approximation of the Dirac function. $\mathbf{n}$ and δ were calculated by Eq. (7) and (8), respectively:

$$\mathbf{n} = \frac{\nabla\phi}{|\nabla\phi|} \quad (7)$$

$$\delta = 6|\nabla\phi||\phi(1-\phi)| \quad (8)$$

The electric force $\boldsymbol{F}_\mathbf{E}$ was calculated by the divergence of the Maxwell stress tensor (Eq. (9)), and the electric field intensity $\boldsymbol{E}$ was obtained by the charge conservation equation (Eq. (11)):

$$\mathbf{F}_\mathbf{E} = \nabla \cdot (\varepsilon(\phi)\mathbf{E}\mathbf{E}^{\mathrm{T}} - \frac{1}{2}\varepsilon(\phi)(\mathbf{E}\cdot\mathbf{E})\mathbf{I}) \quad (9)$$

$$\varepsilon(\phi) = \varepsilon_{\mathrm{w}} + (\varepsilon_{\mathrm{o}} - \varepsilon_{\mathrm{w}})\phi \tag{10}$$

$$\nabla(\sigma(\phi)\mathbf{E} + \varepsilon(\phi)\frac{\partial \mathbf{E}}{\partial \mathrm{t}}) = 0 \tag{11}$$

$$\sigma(\phi) = \sigma_{\mathrm{w}} + (\sigma_{\mathrm{o}} - \sigma_{\mathrm{w}})\phi \tag{12}$$

where ε_{w} and ε_{o} are the permittivity of water and oil, respectively, and σ_{w} and σ_{o} are the conductivities of water and oil, respectively.

In this approach, the Level-Set function was initialized as a distance function (Osher et al., 2003) as follows:

$$\phi = \frac{1}{1 + \mathrm{e}^{\pm \mathrm{D_{si}}/\xi}} \tag{13}$$

where D_{si} is the distance between the initial interface and the nodes of the computational domain. Since the Level-Set function ϕ moves with the fluid, the distance function fluctuates and the interface thickness thus varies. Therefore, re-initialization was needed in order to keep the thichness constant. The numerical stabilization was determined by the parameter λ in Eq. (1). For our case, the secondary droplet volume remained almost constant in a wide λ range of 0.4-1.4 m s^{-1}, and λ=0.6 m s^{-1} was thus used in our calculations. The parameter ξ significantly influences the interface thickness, which is strictly related to mesh refinement, i.e. $h_{\max}/D$. The maximum grid size should be larger than ξ/D, which is quite critical when ξ/D is small. Otherwise, convergence problems occur or the formation of some very fine droplets cannot be reproduced. In the present work, ξ/D=0.03 and $h_{\max}/D$=0.03 were used for all calculations, in which case the model correctly predicted both the progeny droplet volume and the

coalescence kinetics (Vivacqua et al., 2016).

3. Results

3.1 Experimental validation

In order to assess the accuracy of the present model, validation work was conducted with the experimental measurements of V_r ($\frac{\text{Volume}_{\text{secondary}}}{\text{Volume}_{\text{initial}}}$), which was calculated by Eq. (14) for $0 \leq \varnothing \leq 0.5$, as a function of the initial droplet size obtained by Mousavichoubeh et al. (Mousavichoubeh et al., 2011b). The numerical and experimental results are compared in Fig. 2 (a), where a good quantitative agreement was observed. The electric field strength E=373 V mm^{-1} (direct current electric field), and the fluids properties measured by Mousavichoubeh et al. (Mousavichoubeh et al., 2011b) are given in Table 2. In addition, the accuracy of the pressure predictions of the present work was validated by the numerical work of Teigen et al. (TEIGEN et al., 2006), as shown in Fig. 2 (b), where a good qualitative agreement of both droplet behavior and pressure field distribution was obtained.

$$V_r = \frac{\int_{\Omega drop}(1-\varnothing)d\Omega|t_{final}}{\int_{\Omega drop}(1-\varnothing)d\Omega|t_0} \qquad (14)$$

<Table 2 Physical properties of the emulsion>

<Fig. 2: (a) Calculated volume of the secondary droplet obtained by simulation (■) and experiment (☆) (Mousavichoubeh et al., 2011b) work. The parameters of the numerical simulation work were identical to the experimental values (E=373 V mm^{-1}, direct current electric field, γ=0.025 N m^{-1}); (b) A contour plot of the pressure field distribution with an electric field obtained from the literature (Teigen et al., 2006) and the present simulation. The parameters of the numerical simulation work were identical to those of the literature: D=1.1 mm, Bo=0.0959, Oh=0.00417, and Be=0.1, where $Bo = \frac{|\rho_1 - \rho_2| g D^2}{\sigma}$, $Oh = \frac{\mu}{\sqrt{\rho \gamma D}}$, and $Be = \frac{\varepsilon_1 \varepsilon_0 D}{\sigma} E_0^2$.>

3.2 Drop-interface electrocoalescence modes

The elctrocoalescence events of water droplets at an oil/water interface are shown in the sequence of images in Figs. 3, 4, and 5, corresponding to complete coalescence, partial coalescence, and non-coalescence, respectively. Though the above three coalescence mechanisms were experimentally investigated by some researchers (Huo et al., 2015; Mousavi et al., 2014; Mousavichoubeh et al., 2011a; Ristenpart et al., 2009; Wang et al., 2014), a new mode was obtained in the present work, i.e. break-up of bouncing-off droplet non-coalescence(Fig. 5(b)).

Charles et al. (Charles and Mason, 1960) investigated the coalescence of a drop resting on the interface in the absence of external electric

fields, and the results well agreed with the Rayleigh instability theory. Applying external electric fields, deformation of the drop and interface occurred (Fig. 5(a), t=3 ms) due to the polarization. The drop-interface approach was enhanced, and at the instant of contact the electroclamping phenomenon became operative (Ghadiri et al., 2006) giving rise to the formation of a column ((Fig. 5(a), t=4 ms)), i.e. the necking process (Mousavichoubeh et al., 2011a; Mousavichoubeh et al., 2011b). Droplets acquire charges with the same sign as the water phase and experience a Coulomb repulsive force (Atten and Aitken, 2010), which results in partial coalescence. Recently, more attention has been devoted to the influence of capillary pressure on the coalescence process (Bartlett et al., 2015; Lu et al., 2016; Luo et al., 2018; Ristenpart et al., 2009). Moreover, surface tension will push the liquid inside the interface into the water phase via the enlarging column (Fig. 3 (a), t=3-5 ms; Fig. 4(a), t=3-6 ms), i.e. the pumping process (Mousavichoubeh et al., 2011a; Mousavichoubeh et al., 2011b). Coalescence will reduce the system's energy by minimizing the total surface area and corresponding surface energy (Gennes et al., 2004; Ristenpart et al., 2009).

Bird et al. (Bird et al., 2009) reported that the drop and the interface become unstable and rapidly converge below a critical separation distance (d), which is shown in Fig. 3(a). The mode of complete coalescence with upheaval (Aryafar and Kavehpour, 2007) is shown in Fig. 3(b). In this case, the droplet experienced a strong necking process (Fig. 3(b), t=14 ms) and was unstable, where any disturbance, e.g. increasing external electric field strength, decreasing Ohnesorge number ($\mathrm{Oh} = \frac{\mu}{\sqrt{\rho\gamma D}}$), increasing conductivity and permittivity, or increasing drop-interface separation

distance, can result in mode transition to partial coalescence (Fig. 4(a)). With respect to the typical complete coalescence, the upper part of the cone was slightly narrower than the neck of the cone at the instant prior to complete coalescence (Fig. 3 (a), t=10 ms). However, for upheaval complete coalescence, the upper part of the cone prior to complete coalescence was wider than the neck of the cone (Fig. 3 (b), t=14 ms), which is similar with typical partial coalescence ((Fig. 4 (a), t=12 ms)). When typical partial coalescence takes place, the primary droplet does not entirely merge into the water phase and progeny droplets, and generally one main droplet and a few much finer ones (Fig. 4(a), t=21 ms), are formed. Fig. 4(b) shows a strong partial coalescence pattern, i.e. jet-like partial coalescence. In this case, the secondary droplet experienced disintegration into further fine progeny droplets, which is very undesirable in terms of emulsion separation performance. Moreover, as is shown in Fig. 4(b) (t=8 and 14 ms), fine secondary droplets were formed at the top of the main secondary droplets, which was also observed by Mousavichoubeh (Mousavichoubeh et al., 2011b). The conical shape (Fig. 3(a), t=12 ms; Fig. 3(b), t=22 ms) is often referred to as a Taylor cone (Ristenpart et al., 2009; Taylor, 1964).

<Fig. 3 Time evolution of drop-interface complete coalescence: (a) Typical complete coalescence: E=373 V mm^{-1}, D=1.196 mm; σ_w=5.49×10^{-5} S m^{-1}; ε_o=1; γ=0.025 N m^{-1}, d=0.1 mm; (b) Complete coalescence with upheaval: E=373 V mm^{-1}, D=1.196 mm; σ_w=5.49×10^{-3} S m^{-1}; ε_o=3;

γ=0.025 N m^{-1}, drop-interface distance (d)=0.1 mm. The fluids properties are given in Table 2.>

<Fig. 4 Time evolution of drop-interface partial coalescence: (a) Typical partial coalescence: E=373 V mm^{-1}, D=1.196 mm; σ_w=5.49×10^{-5} S m^{-1}; γ=0.025 N m^{-1}, d=0.1 mm; (b) Jet-like partial coalescence: E=373 V mm^{-1}, D=1.196 mm; σ_w=5.49×10^{-4} S m^{-1}; γ=0.025 N m^{-1}, d=0.1 mm. The fluids properties are given in Table 2.>

Non-coalescence modes are shown in Fig. 5. When the distance between the droplet and interface is sufficiently close, electrical stresses deform the leading edges of the drop and the interface into a double cone (Bird et al., 2009) (Fig. 5(a), t= 3 ms). Reaching a critical distance, the local electric field strength in the gap rapidly increased and a narrow liquid bridge (Fig. 5(a), t= 4 ms) was formed. After a short period of bridge enlargement (Fig. 5(a), t= 4-6 ms), the bridge thickness was reduced (Fig. 5(a), t= 6-8 ms), and non-coalescence occurred. Mousavi et al. (Mousavi et al., 2014) proposed that the non-coalescence was resulted from the inability of the surface tension force to overcome the electrostatic force. The feature formed in Fig. 5(b) is interesting and requires analysis to determine what processes gave rise to this mode. Following the formation of a very thin bridge (Fig. 5(b), t=6 ms) between the droplet and interface, the droplet strangely deformed, i.e. an ellipsoid with a sharp top and a

circular bottom, which is different from the typical non-coalescence (Fig. 5(a)). The droplet was then stretched into a symmetrical spindle (Fig. 5(b), t=13 ms). When the deformation ratio reached a critical value, the bouncing-off droplet broke into two main droplets and a number of fine ones (Fig. 5(b), t=30 ms). Moreover, very fine progeny droplets were formed at the top of the mother one as well.

<Fig. 5 Time evolution of drop-interface non-coalescence: (a) Typical non-coalescence: E=373 V mm^{-1}, D=0.984 mm; σ_w=5.49×10^{-3} S m^{-1}; γ=0.025 N m^{-1}, d=0.15 mm; (b) Breakup of bouncing-off droplet non-coalescence: E=373 V mm^{-1}, D=1.196 mm; σ_w=5.49×10^{-5} S m^{-1}; γ=0.025 N m^{-1}, d=0.2 mm. The fluids properties are given in Table 2.>

4. Discussion

4.1 Pressure field distribution

The electric field determines the distortion of the drop and the oil/water meniscus prior to contact, while the subsequent coalescence dynamics predominantly depend on capillarity (Bird et al., 2009). The coalescence process of the liquid bridge is significantly influenced by the mean curvature of the interface which is related to the capillary pressure (Bartlett et al., 2015; Luo et al., 2018). Moreover, the velocity vortex, which significantly affects the charge transfer mechanism and secondary droplet size, is generated by the mismatch in capillary pressure (Hamlin et al.,

2012). The underlying physics of the effects of capillary pressure, such as the pressure field distribution on the electrocoalescence are not completely understood, although some literatures (Bartlett et al., 2015; Luo et al., 2018; Ristenpart et al., 2009) have addressed it qualitatively by the Young-Laplace equation as follows.

$$\Delta p = p_{\mathrm{drop}} - p_{\mathrm{bridge}} = \frac{2\gamma}{R} - \frac{\gamma}{r_{\mathrm{m}}}(1 - \cot\theta) \qquad (15)$$

where R is the droplet radius, r_{m} is the liquid bridge radius, γ is the oil/water interfacial tension, and θ is the double-cone angle. Therefore, the effects of the pressure gradient on the electrocoalescence mode transition deserve to be intensively discussed.

The time-lapsed evolution of the pressure field of the complete coalescence mode is shown in Fig. 6. Then, the capillary pressure was always negative until t=12 ms. From the Fig. 6(a), it can be seen that at the instant of the application of external electric field (t=0-1 ms), the sign of the pressure inside the droplet changed to the opposite one. The pressure includes charge induced pressure and interfacial tension induced pressure whose balance is quantified by the non-dimensional electrocapillary number, $\epsilon_c = \frac{\varepsilon\varepsilon_0 E^2 R}{\gamma}$, where $\varepsilon\varepsilon_0$ is the permittivity of the liquid, E is the magnitude of the electric field, R is the radius of the drop, and γ is the surface tension (Bird et al., 2009). Therefore, the pressure field is predominantly determined by the coupling effect of the surface tension (curvature) and electric field. The underlying dynamics of the sign change of the pressure field will be investigated further and are not discussed in the present work. In addition, the pressure of the droplet was higher than

that of the liquid bridge ($\Delta p>0$), and the top of the droplet had the highest pressure. In contrast, Fig. 6(b) shows that the capillary pressure was always positive (t>7 ms) during the complete coalescence with upheaval. Moreover, the upheaval had a large positive capillary pressure. Nevertheless, the Δp was larger than zero in the whole process, which is consistent with typical complete coalescence. Some researchers (Bartlett et al., 2015; Lu et al., 2016) conducted theoretical investigations of the bridge model and reported that the system presents coalescence when the bridge pressure is negative. However, from the present work, the pressure gradients between the drop and the bridge rather than the sign of the pressure determined the coalescence. The pressure gradients in the liquid can drive fluid motion as the liquid rearranges and the bridge grows. It is noteworthy that the large positive pressures (Fig. 6(a), t=12 ms; Fig. 6(b), t=19 ms) in the conical tip, which led to the pressure gradient from the conical tip (positive pressure) to the upper oil phase (negative pressure), contributed to the formation of fine secondary droplets, which was experimentally observed by Mousavichoubeh et al (Mousavichoubeh et al., 2011b). The pressure conditions that led to the formation of the conical tip resulted from the imbalance of the charge induced pressure and interfacial tension induced pressure (Bird et al., 2009). In addition, in the regions of small curvature, the pressure in the water (lower) phase was slightly larger than that in the oil (upper) phase near the interface at t=10 and 12 ms in Fig. 6 (not shown for brevity).

<Fig. 6 Evolution of the pressure field distribution in the complete coalescence mode: (a) Typical complete coalescence: E=373 V mm^{-1}, D=1.196 mm; σ_w=5.49×10^{-5} S m^{-1}; ε_o=1; γ=0.025 N m^{-1}, d=0.1 mm; (b) Complete coalescence with upheaval: E=373 V mm^{-1}, D=1.196 mm; σ_w=5.49×10^{-3} S m^{-1}; ε_o=3; γ=0.025 N m^{-1}, d=0.1 mm. The fluids properties are given in Table 2.>

Fig. 7 illustrates the evolution of the pressure field distribution in the partial coalescence mode. From Fig. 7, it was found that at the early contact period (t≤2 ms), though Δp>0, the pressure in the drop was negative. The thickness of the liquid bridge rapidly increased, and the liquid in the drop was squeezed to the bulk phase. However, at t=15 ms, the pressure in the liquid bridge started to become larger than that in the drop (Δp<0). The flow was forced in the reverse direction, i.e. from the liquid bridge to the drop, and the oil/water interface broke up due to the Rayleigh-Plateau instability (Bartlett et al., 2015) (t=17 ms). In addition, the capillary pressure of the main secondary droplet tail was very high (t=18 ms), which may be the reason for the formation of fine progeny droplets (t=20 ms), e.g. secondary breakup. In order to verify the above hypothesis, the pressure field distribution of the jet-like partial coalescence (t=26 ms) is given in Fig. 8. From the figure, it can be seen that the very high capillary pressure in the tail region resulted in the fine progeny droplets (t=30 ms) shown in Fig. 4(b).

<Fig. 7 Evolution of the pressure field distribution in the typical partial coalescence mode. The calculation conditions were: E=373 V mm^{-1}, D=1.196 mm; σ_w=5.49×10^{-5} S m^{-1}; γ=0.025 N m^{-1}, d=0.1 mm and fluids properties are given in Table 2.>

<Fig. 8 The pressure field distribution at t=26 ms in the Jet-like partial coalescence mode. The calculation conditions were: E=373 V mm^{-1}, D=1.196 mm; σ_w=5.49×10^{-4} S m^{-1}; γ=0.025 N m^{-1}, d=0.1 mm and fluids properties are given in Table 2.>

The time evolution of the pressure field distribution shown in Fig. 9 illustrates that the capillary pressure in the drop and bridge was positive in the whole process. Bird et al. (Bird et al., 2009) reported that the bridge region has the largest deformations of a self-similar shape, which is consistent with the present work. The bridge thickness increased from the moment of contact to t=6 ms and then decreased until bouncing off. Interestingly, though the capillary pressure in the bridge was always higher than the drop, the droplets did not immediately bounce off, which may be because of the approach velocity. With increasing Δp, the bridge thickness decreased such as t=6-8 ms. The largest pressure was at 8 ms, after which bouncing off occurred. In addition, the droplet deformation ratio continuously increased in the non-coalescence and the Taylor cone occurred at the bouncing off process (t=9 ms). Fig. 8 illustrates that the secondary breakup occurred in the region of high capillary pressure, which was also

observed in the breakup of the bouncing-off droplet non-coalescence mode (Fig. 9 (b)).

<Fig. 9 Evolution of the pressure field distribution in the non-coalescence mode. (a) Typical non-coalescence: E=373 V mm^{-1}, D=0.984 mm; σ_w=5.49×10^{-3} S m^{-1}; γ=0.025 N m^{-1}, d=0.15 mm; (b) Breakup of bouncing-off droplet, t=25 ms: E=373 V mm^{-1}, D=1.196 mm; σ_w=5.49×10^{-5} S m^{-1}; γ=0.025 N m^{-1}, d=0.2 mm. The fluids properties are given in Table 2.>

4.2 Drop-interface electrocoalescence mode transition

Mousavi et al. (Mousavi et al., 2014) and Mousavichoubeh et al. (Mousavichoubeh et al., 2011a; Mousavichoubeh et al., 2011b) reported that at a high electric field (E) or large droplet size (D), partial coalescence could occur. However, in the present work, partial coalescence and non-coalescence can occur at the same E (373 V mm^{-1}) and D (1.196 mm) with complete coalescence. Therefore, the drop-interface electrocoalescence mode transition needs to be assessed in depth. Vivacqua et al. (Vivacqua et al., 2016) reported that a closer initial drop-interface distance determines a smaller contact angle formed between the drop and the layer surface, which is beneficial to complete coalescence (Bartlett et al., 2015; Bird et al., 2009; Luo et al., 2018). Pillai et al. (Pillai et al., 2015) also predicted that a larger drop-interface distance promotes non-coalescence. The

results of a number of simulations (Fig. 10) showed that there is a critical non-dimensional drop-interface distance (d/D, where d is the drop-interface distance and D is the initial droplet diameter) of electrocoalescence modes that have negligible dependence on the non-dimensional water phase conductivity (σ_w/σ_{ini}, where $\sigma_{ini}=5.49\times10^{-6}$ S m^{-1}). From Fig. 10, it was found that a large distance, corresponding to $d/D\geq0.15$, led to non-coalescence, while a small distance, corresponding to $d/D\leq0.08$, led to complete drop-interface coalescence. At $0.08<d/D<0.15$, partial coalescence occurred. The reason may be that a large distance results in a large kinetic energy of the droplet approaching the interface, which prevents the occurrence of complete coalescence (Vivacqua et al., 2016). In addition, from Fig. 10, it was found that the coalescence mode transition was independent of conductivity, which is consistent with the experimental results by Hamlin et al (Hamlin et al., 2012). Though the conductivity has negligible effects on the transition of coalescence modes, it affects the secondary droplet size of partial coalescence in terms of the charge transfer mechanism (Vivacqua et al., 2016). Mousavichoubeh et al. (Mousavichoubeh et al., 2011b) reported that upon contact of a neutral (but polarized) drop with a negatively charged interface, the drop becomes negatively charged via a connecting bridge and obtains an electric repulsive force from the interface, which was numerically observed in the present work (Fig. 11).

<Fig. 10 Simulations are shown for a range of non-dimensional drop-interface distances and non-dimensional water phase conductivity.

The red dashed lines are shown to highlight the critical non-dimensional distance.>

<Fig. 11 Electrostatic force and space charge density (C m^{-3}) in the coalescence region after 5 ms. The calculation conditions were: σ_w=5.49×10^{-6} S m^{-1}, E=373 V mm^{-1}, D=1.196 mm, d=0.1 mm. The fluids properties are given in Table 2.>

The current state of understanding (Li et al., 2017c; Mousavichoubeh et al., 2011b; Vivacqua et al., 2016) points to two dimensionless groups, the electrical Weber Number, $\mathrm{We} = \frac{\varepsilon_0 \varepsilon_{\mathrm{oil}} E^2 D}{\gamma}$, accounting for the intensification of the necking process, and the Ohnesorge Number, $\mathrm{Oh} = \frac{\mu}{\sqrt{\rho \gamma D}}$, accounting for the rate of pumping. The partial coalescence process is a competing process between the electrostatic stress and interfacial tension, and its pumping rate is affected by the bulk viscosity. Therefore, the coupling effects of We and Oh on V_r ($\frac{\mathrm{Volume_{secondary}}}{\mathrm{Volume_{initial}}}$) can be described with the following combination of these two dimensionless numbers:

$$\mathrm{We/Oh} = \frac{\rho^{0.5} \varepsilon_0 \varepsilon_{\mathrm{oil}} E^2 D^{1.5}}{\mu_{\mathrm{oil}} \gamma^{0.5}} \qquad (16)$$

For a range of electric field strengths (116-450 V mm^{-1}), droplet sizes (0.829-1.500 mm), oil relative permittivity (1.0-4.9), surface tensions (0.015-0.050 N m^{-1}), and bulk viscosities (35.0-61.5 mPa s) as given in Table 3, V_r as a function of We/Oh is shown in Fig. 12, where a good power

function trend, which is given by Eq. (17), was obtained with data of all the conductivities. The V_r values of 0 and 1 corresponds to non-coalescence and complete coalescence, respectively, and the other values (0-1) mean partial coalescence. Hence, the new dimensionless number reasonably well predicts the formation of secondary droplets and coalescence modes, considering the range of parameters used in Table 3. In addition, from Fig. 12, V_r first increased and then decreased with increasing conductivities, which was also reported by Vivacqua et al (Vivacqua et al., 2016). In summary to enhance complete coalescence, the We/Oh Number needs to be optimized for a given oil-water system through electrocoalescer design and operation.

$$V_r = a \cdot (\mathrm{We/Oh} \times 10^3)^b \qquad (17)$$

where a and b are constants. Particularly, at $\sigma_w/\sigma_{ini}=1$, $a_1=3.62\times10^{-20}$, $b_1=6.43$ (R-squared=0.96); at $\sigma_w/\sigma_{ini}=10$, $a_2=1.17\times10^{-17}$, $b_2=5.74$ (R-squared=0.95); at $\sigma_w/\sigma_{ini}=100$, $a_3=8.27\times10^{-13}$, $b_3=4.15$; (R-squared=0.97); at $\sigma_w/\sigma_{ini}=1000$, $a_4=7.75\times10^{-17}$, $b_4=5.47$ (R-squared=0.96).

<Fig. 12 Calculated volume of the secondary droplet as a function of the We/Oh number. The data points were calculated values for conductivity of $\sigma_w/\sigma_{ini}=1$ (□), $\sigma_w/\sigma_{ini}=10$ (○), $\sigma_w/\sigma_{ini}=100$ (△), and $\sigma_w/\sigma_{ini}=1000$ (☆). The lines are fitted trend lines.>

<Table 3 Parameters used in the We/Oh number calculation>

5. Conclusions

The electrocoalescence process of an aqueous droplet with a planar interface in the presence of externally direct current electric fields was analyzed with the Level-Set method describing the interface. The effects of the electric field strength, droplet size, oil phase permittivity, surface tension, bulk viscosity, water phase conductivity, and drop-interface distance were assessed. Good agreement was obtained between numerical and experimental results in the literature, indicating that the model is capable of reproducing drop-interface electrocoalescence under direct current electric fields. Three coalescence modes were obtained: complete coalescence, including typical complete coalescence and complete coalescence with upheaval; partial coalescence, including typical partial coalescence and jet-like partial coalescence; and non-coalescence, including typical non-coalescence and breakup of the bouncing-off droplet non-coalescence. The pressure gradients between the drop and the bridge rather than the sign of the pressure determine the coalescence. The very high capillary pressure of the main secondary droplet tail results in secondary breakup, which is undesirable in terms of emulsion separation performance. There is a critical non-dimensional drop-interface distance of electrocoalescence modes that has negligible dependence on the non-dimensional water phase conductivity.

The drop-interface electrocoalescence process is a competing process between the electrostatic stress and interfacial tension, determined by the coupling effects of the Weber Number and the Ohnesorge Number. The ratio We/Oh was found to well describe the electrocoalescence process. This will be useful for optimizing the design of the electrocoalescence systems in a generic way, accounting for the liquids properties, electrode configuration, geometry, and applied electric potential.

Acknowledgments

The financial support of National Natural Science Foundation of China (No. 51761145011, and No. 51506078), China Scholarship Council (No. 201606450040), and State Key Laboratory of Heavy Oil Processing (SLKZZ-2017013) for supporting the first author to carry out the research work at the University of Leeds is gratefully acknowledged.

References

Aryafar, H., Kavehpour, H.P., 2009. Electrocoalescence: effects of DC electric fields on coalescence of drops at planar interfaces. Langmuir 25, 12460-12465.

Aryafar, H., Kavehpour, H.P., 2010. Electrocoalescence fireworks. Physics of Fluids 22.

Aryafar, H., Kavehpour, P.J.P.o.F., 2007. Electrocoalescence. 19, 091107.

Atten, P., Aitken, F.J.I.T.o.I.A., 2010. Electrocoalescence criterion for two close anchored water drops and estimate for pairs of drops in a field. IEEE Transactions on Industry Applications 46, 1578-1585.

Bartlett, C.T., Genero, G.A., Bird, J.C.J.J.o.F.M., 2015. Coalescence and break-up of nearly inviscid conical droplets. 763, 369-385.

Bird, J.C., Ristenpart, W.D., Andrew, B., Stone, H.A., %J Physical Review Letters, 2009. Critical angle for electrically driven coalescence of two conical droplets. 103, 164502.
Blanchette, F., Bigioni, T.P.J.J.o.F.M., 2009. Dynamics of drop coalescence at fluid interfaces. Journal of Fluid Mechanics 620, 333-352.
Blanchette, F., Bigioni, T.P.J.N.P., 2006. Partial coalescence of drops at liquid interfaces. Nature Physics 2, 254-257.
Charles, G.E., Mason, S.G.J.J.o.C.S., 1960. The mechanism of partial coalescence of liquid drops at liquid/liquid interfaces. 15, 105-122.
Choi, S.W., Dong, E.L., Lee, W.I., Han, S.K.J.A.S.S., 2016. Analysis of Coalescence Behavior for Compressed Droplets. 397, 57-69.
Collins, R.T., Jones, J.J., Harris, M.T., Basaran, O.A.J.N.P., 2008. Electrohydrodynamic tip streaming and emission of charged drops from liquid cones. 4, 149-154.
Eow, J.S., Ghadiri, M.J.S., technology, p., 2002. Electrocoalesce-separators for the separation of aqueous drops from a flowing dielectric viscous liquid. 29, 63-77.
Eow, J.S., Mojtaba, G.J.C.E.J., 2001. Electrostatic enhancement of coalescence of water droplets in oil: a review of the technology. 84, 173-192.
Gennes, P.G.D., Brochard-Wyart, F., Quéré, D., 2004. Capillarity and Wetting Phenomena.
Ghadiri, M., Martin, C.M., Arteaga, P.A., Tüzün, U., Formisani, B.J.C.E.S., 2006. Evaluation of the single contact electrical clamping force. 61, 2290-2300.
Goto, M., Irie, J., Kondo, K., Nakashio, F.J.J.o.C.E.o.J., 1989. Electrical demulsification of W/O emulsion by continuous tubular coalescer. 22, 401-406.
Hamlin, B., Creasey, J., Ristenpart, W.J.P.r.l., 2012. Electrically tunable partial coalescence of oppositely charged drops. 109, 094501.
Helmensdorfer, S., Topping, P.J.E., 2013. Bouncing of charged droplets: An explanation using mean curvature flow. 104, 34001.
Hirato, T., Koyama, K., Tanaka, T., Awakura, Y., Majima, H.J.M.T., JIM, 1991. Demulsification of water-in-oil emulsion by an electrostatic coalescence method. 32, 257-263.
Holto, J., Berg, G., Lundgaard, L.E., 2009. Electrocoalescence of drops in a water-in-oil emulsion, Electrical Insulation and Dielectric Phenomena, 2009. CEIDP'09. IEEE Conference on. IEEE, pp. 196-199.
Hongmiao, T., Jinyou, S., Yucheng, D., Xin, L., Xiangming, L.J.E., 2011. Numerical studies of electrically induced pattern formation by coupling liquid dielectrophoresis and two-phase flow. 32, 2245-2252.
Huo, Y., Wang, J., Qiu, H., Zuo, Z., Fan, Y.J.E.i.F., 2015. Noncontact rebound and fission of oppositely charged droplets. 56, 65.
Karyappa, R.J.J.o.F.M., 2014. Breakup of a conducting drop in a uniform electric field. 754, 550-589.
Li, B., Fan, Y., Sun, Z., Wang, Z., Zhu, L.J.P.T., 2017a. Effects of high-frequency pulsed electrical field and operating parameters on dehydration of SAGD produced ultra-heavy oil. 316.
Li, B., Fan, Y., Sun, Z., Wang, Z., Zhu, L.J.P.T., 2017b. Effects of high-frequency pulsed electrical field and operating parameters on dehydration of SAGD produced ultra-heavy oil. 316, 338-344.
Li, B., Sun, Z., Wang, Z., Jin, Y., Fan, Y.J.J.o.E., 2016. Effects of high-frequency and high-voltage pulsed electric field parameters on water chain formation. 80, 22-29.
Li, B., Vivacqua, V., Ghadiri, M., Sun, Z., Wang, Z., Li, X., Li, B., Vivacqua, V., Ghadiri, M., Sun, Z.J.C.E.R., Design, 2017c. Droplet Deformation under Pulsatile Electric Fields. 127.

Lu, J., Fang, S., Corvalan, C.M.J.P.R.E., 2016. Coalescence dynamics of viscous conical drops. 93, 023111.
Luo, S., Schiffbauer, J., Luo, T.J.P.C.C.P., 2016. Effect of electric field non-uniformity on droplets coalescence. 18.
Luo, X., Yin, H., Yan, H., Huang, X., Yang, D., He, L.J.C.E.S., 2018. The electrocoalescence behavior of surfactant-laden droplet pairs in oil under a DC electric field. 191, 350-357.
Mhatre, S., Simon, S., Sjöblom, J.J.C.E.R., Design, 2019. Shape evolution of a water drop in asphaltene solution under weak DC electric fields. 141, 540-549.
Mhatre, S., Vivacqua, V., Ghadiri, M., Abdullah, A.M., Al-Marri, M.J., Hassanpour, A., Hewakandamby, B., Azzopardi, B., Kermani, B.J.C.E.R., Design, 2015. Electrostatic phase separation: A review. 96, 177-195.
Mohammed, R.A., Bailey, A.I., Luckham, P.F., Taylor, S.E.J.C., Physicochemical, S.A., Aspects, E., 1994. Dewatering of crude oil emulsions 3. Emulsion resolution by chemical means. 83, 261-271.
Mousavi, S., Ghadiri, M., Buckley, M.J.C.E.S., 2014. Electro-coalescence of water drops in oils under pulsatile electric fields. 120, 130-142.
Mousavichoubeh, M., Ghadiri, M., Shariaty-Niassar, M.J.C.E., Intensification, P.P., 2011a. Electro-coalescence of an aqueous droplet at an oil–water interface. 50, 338-344.
Mousavichoubeh, M., Shariaty-Niassar, M., Ghadiri, M.J.C.e.s., 2011b. The effect of interfacial tension on secondary drop formation in electro-coalescence of water droplets in oil. 66, 5330-5337.
Olsson, E., Kreiss, G., 2005. A conservative level set method for two phase flow.
Osher, S., Fedkiw, R., Piechor, K., 2003. Level Set Methods and Dynamic Implicit Surfaces.
Pillai, R., Berry, J., Harvie, D.J., Davidson, M.R., 2015. Electrophoretic effects on satellite droplet formation during electrocoalescence of microdrops, 11th International Conference on CFD in the Minerals and Process Industries, no.
Pillai, R., Berry, J.D., Harvie, D.J.E., Davidson, M.R., 2017. Electrophoretically mediated partial coalescence of a charged microdrop. Chemical Engineering Science 169, 273-283.
Ristenpart, W.D., Bird, J.C., Belmonte, A., ., Dollar, F., ., Stone, H.A., %J Nature, 2009. Non-coalescence of oppositely charged drops. 109, 384-389.
Rommel, W., Meon, W., Blass, E.J.S.s., technology, 1992. Hydrodynamic modeling of droplet coalescence at liquid-liquid interfaces. 27, 129-159.
Saranin, V.A.J.J.o.E., Physics, T., 2011. On the theory of the noncoalescence effect for oppositely charged droplets. 112, 896-901.
Sethian, J.A., 1999. Level set methods and fast marching methods: evolving interfaces in computational geometry, fluid mechanics, computer vision, and materials science. Cambridge university press.
Shadloo, M., S., Rahmat, Mechanics, Y.J.C., 2013. A smoothed particle hydrodynamics study on the electrohydrodynamic;deformation of a droplet suspended in a neutrally buoyant Newtonian;fluid. 52, 693-707.

Sun, D., Chung, J.S., Duan, X., Ding, Z.J.C., Physicochemical, S.A., Aspects, E., 1999. Demulsification of water-in-oil emulsion by wetting coalescence materials in stirred- and packed-columns. 150, 69-75.

Taylor, G.J.P.o.t.R.S.o.L., 1964. Disintegration of Water Drops in an Electric Field. 280, 383-397.

Taylor, S.J.C.e.r., design, 1996. Theory and practice of electrically-enhanced phase-separation of water-in-oil emulsions. 74, 526-540.

TEIGEN, K.E., MUNKEJORD, S.T., BJØRKLUND, E., 2006. A computational study of the coalescence process between a drop and an interface in an electric field, CFD2008-6th International Conference on Computational Fluid Dynamicics in the Oil and Gas, Metallurgical and Process Industries (Trondheim, Norway, 2008).

Vivacqua, V., Ghadiri, M., Abdullah, A.M., Hassanpour, A., Al-Marri, M.J., Azzopardi, B., Hewakandamby, B., Kermani, B.J.C.E.R., Design, 2016. ANALYSIS OF PARTIAL ELECTROCOALESCENCE BY LEVEL-SET AND FINITE ELEMENT METHODS. 114, 180-189.

Vivacqua, V., Mhatre, S., Ghadiri, M., Abdullah, A., Hassanpour, A., Al-Marri, M., Azzopardi, B., Hewakandamby, B., Kermani, B.J.C.E.R., Design, 2015. Electrocoalescence of water drop trains in oil under constant and pulsatile electric fields. 104, 658-668.

Wang, J., Wang, B., Qiu, H.J.S.r., 2014. Coalescence and breakup of oppositely charged droplets. 4, 7123.

Wang, Z., Dong, K., Tian, L., Wang, J., Tu, J., 2018. Numerical study on coalescence behavior of suspended drop pair in viscous liquid under uniform electric field. AIP Advances 8.

Xin, H., He, L., Luo, X., Yang, D., Shi, K., Yan, H.J.I.J.o.M.F., 2017. Breakup mode transformation of leaky dielectric droplet under direct current electric field. 96, 123-133.

Yu, K., Zhang, H., Biggs, S., Xu, Z., Cayre, O.J., Harbottle, D., 2018. The rheology of polyvinylpyrrolidone-coated silica nanoparticles positioned at an air-aqueous interface. J Colloid Interface Sci 527, 346-355.

Yue, P., Zhou, C., Feng, J.J.J.P.o.F., 2006. A computational study of the coalescence between a drop and an interface in Newtonian and viscoelastic fluids. 18, 105-126.

Table 1 The conclusions of the numerical literatures and the novelty of the present work

Literatures	Conclusions and differences		Novelty of the present work
Blanchette and Bigioni, 2006 Yue et al., 2006 Blanchette and Bigioni, 2009	➢ Literature: Air surroundings ➢ Present work: Liquid surroundings ➢ Literature: Viscoelasticity ➢ Present work: Capillary pressure.	Partial coalescence without an electric field	➢ Providing another insight from a viewpoint of capillary pressure ➢ Finding new drop-interface coalescence modes ➢ Developing a scaling relation for the normalized volume of the secondary droplet as a function of the coupling effect of electric and physical parameters ($V_r=a\cdot(We/Oh\times10^3)^b$)
Teigen et al., 2006	➢ Literature: Without considering charge relaxation ➢ Present work: With considering charge relaxation	Partial coalescence with an electric field	
Hongmiao et al., 2011	➢ Literature: Geometry ➢ Present work: Capillary pressure		
Karyappa et al., 2014	➢ Literature: Process prior to pinch-off ➢ Present work: Whole process		
Vivacqua et al., 2016	➢ Literature: Accuracy improvement of the model ➢ Present work: The mechanism for mode transformation		
Pillai et al., 2017	➢ Literature: Charge transfer dynamics		

➢ Present work: Capillary pressure	

Table 2 Physical properties of the emulsion

Liquid	Conductivity (μs m^{-1}) (±5%)	Viscosity (mPa s)	Density (kg m^{-3})	Dielectric constant
Deionised water	5.49	1.0	1000	80.0
Sunflower oil	7.62×10^{-5}	46.5	922	4.9

10 **Table 3 Parameters used in the We/Oh number calculation**

We/Oh ($\times 10^3$)	Electric field strength (V mm^{-1})	Droplet diameter (mm)	Oil relative permittivity	Surface tension (N m^{-1})	Oil Viscosity (mPa s)
70.5	116	1.196	4.9	0.025	46.5
148.7	373	1.196	1.0	0.025	46.5
181.2	186	1.196	4.9	0.025	46.5
253.5	220	1.196	4.9	0.025	46.5
265.2	225	1.196	4.9	0.025	46.5
297.5	373	1.196	2.0	0.025	46.5
343.3	256	1.196	4.9	0.025	46.5
420.5	373	0.829	4.9	0.025	46.5
446.2	373	1.196	3.0	0.025	46.5
515.3	373	1.196	4.9	0.050	46.5
543.8	373	0.984	4.9	0.025	46.5
551.0	373	1.196	4.9	0.025	61.5
556.7	326	1.196	4.9	0.025	46.5
576.1	373	1.196	4.9	0.040	46.5
594.9	373	1.196	4.0	0.025	46.5
599.8	373	1.196	4.9	0.025	56.5
615.9	373	1.196	4.9	0.035	46.5
642.8	373	1.100	4.9	0.025	46.5
652.7	353	1.196	4.9	0.025	46.5
658.0	373	1.196	4.9	0.025	51.5
665.3	373	1.196	4.9	0.030	46.5
690.2	363	1.196	4.9	0.025	46.5
728.8	373	1.196	4.9	0.025	46.5
768.4	383	1.196	4.9	0.025	46.5
809.0	393	1.196	4.9	0.025	46.5
814.8	373	1.196	4.9	0.020	46.5
816.6	373	1.196	4.9	0.025	41.5
850.7	403	1.196	4.9	0.025	46.5
893.4	413	1.196	4.9	0.025	46.5
928.4	373	1.196	4.9	0.025	36.5

940.8	373	1.196	4.9	0.015	46.5
968.2	373	1.196	4.9	0.025	35.0
1023.6	373	1.500	4.9	0.025	46.5
1060.7	450	1.196	4.9	0.025	46.5

11

12

13

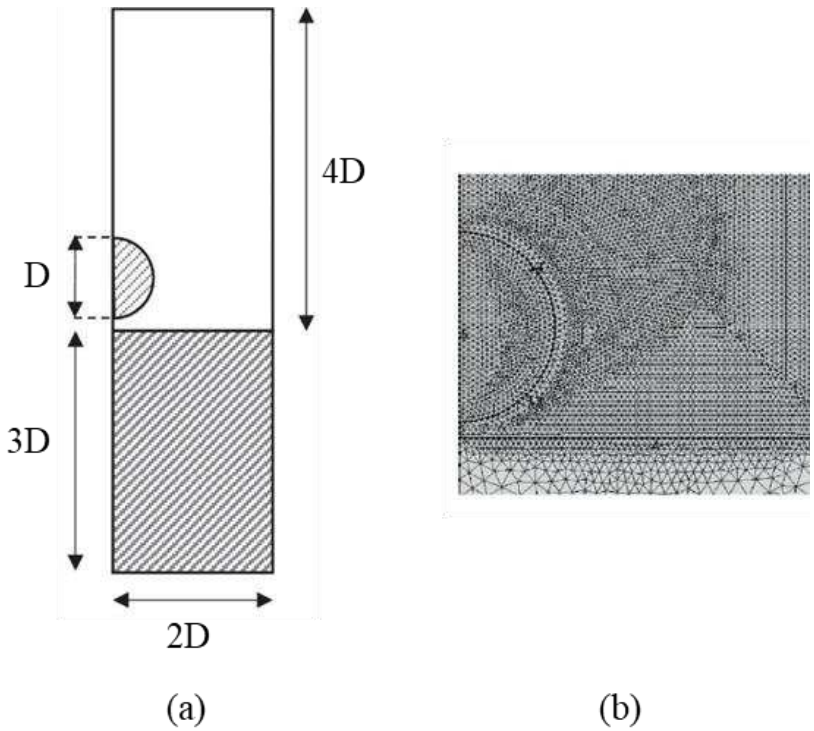

Fig. 1 (a) Sketch of the simulation domain. (b) Close-up of the mesh for h_{max}/D=0.03.

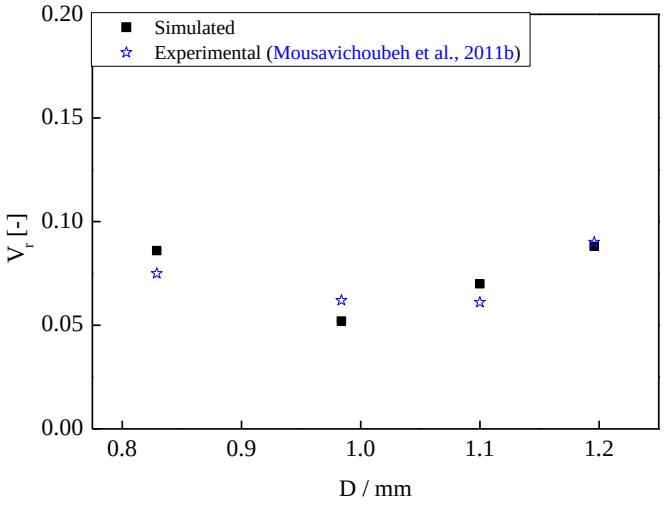

(a)

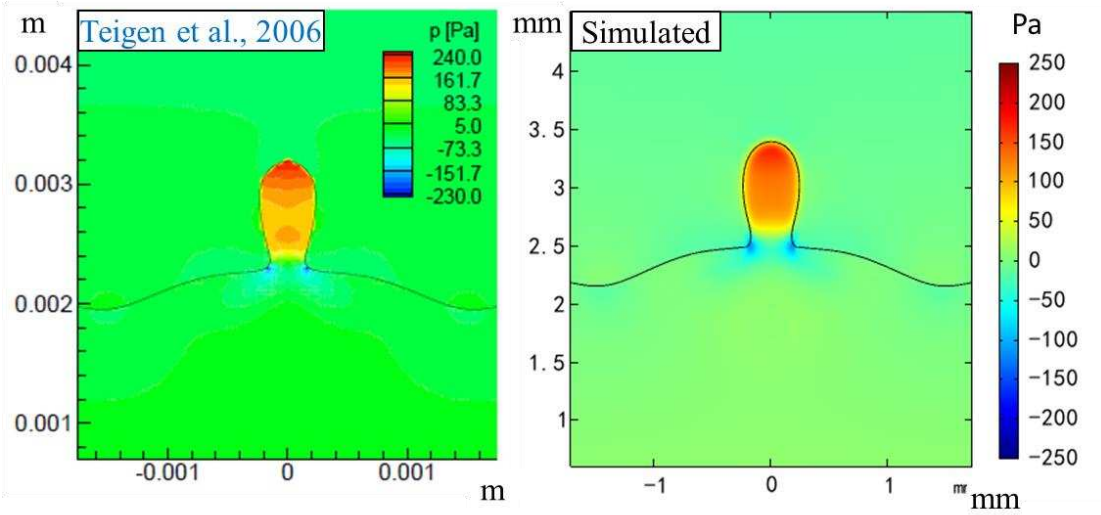

(b)

Fig. 2: (a) Calculated volume of the secondary droplet obtained by simulation (■) and experiment (☆) (Mousavichoubeh et al., 2011b) work. The parameters of numerical simulation work are identical to the experimental values (*E*=373 V mm^{-1}, direct current electric field, γ=0.025 N m^{-1}); (b) Contour plot of the pressure field distribution with an electric field obtained from the literature (Teigen et al., 2006) and the present simulation. The parameters of the numerical simulation work are identical to the literature: *D*=1.1 mm, *Bo*=0.0959, *Oh*=0.00417, and *Be*=0.1, where $\boldsymbol{Bo = \frac{|\rho_1-\rho_2|gD^2}{\sigma}}$, $\boldsymbol{Oh = \frac{\mu}{\sqrt{\rho\gamma D}}}$, **and** $\boldsymbol{Be = \frac{\varepsilon_1\varepsilon_0 D}{\sigma}E_0^2}$.

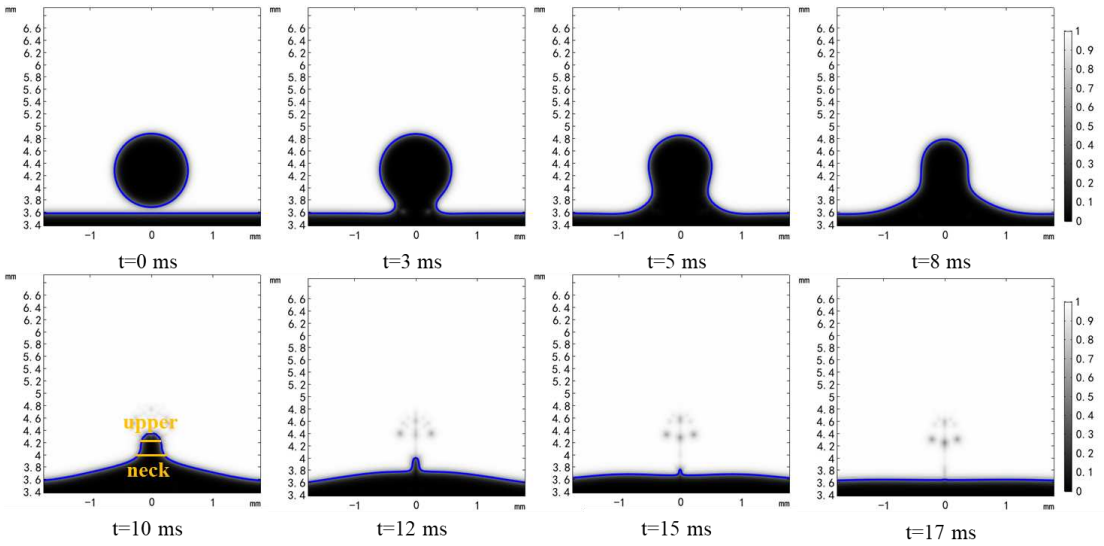

(a)

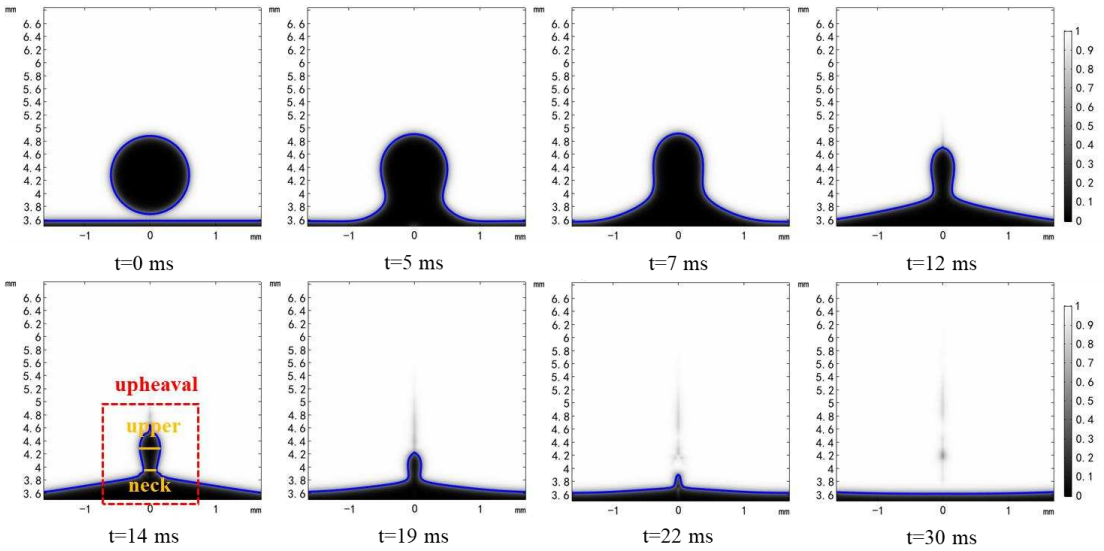

(b)

Fig. 3 Time evolution of the drop-interface complete coalescence: (a) Typical complete coalescence: E=373 V mm^{-1}, D=1.196 mm; σ_w=5.49×10^{-5} S m^{-1}; ε_o=1; γ=0.025 N m^{-1}, d=0.1 mm; (b) Complete coalescence with upheaval: E=373 V mm^{-1}, D=1.196 mm; σ_w=5.49×10^{-3} S m^{-1}; ε_o=3; γ=0.025 N m^{-1}, drop-interface distance (d)=0.1 mm. The fluids properties are given in Table 2.

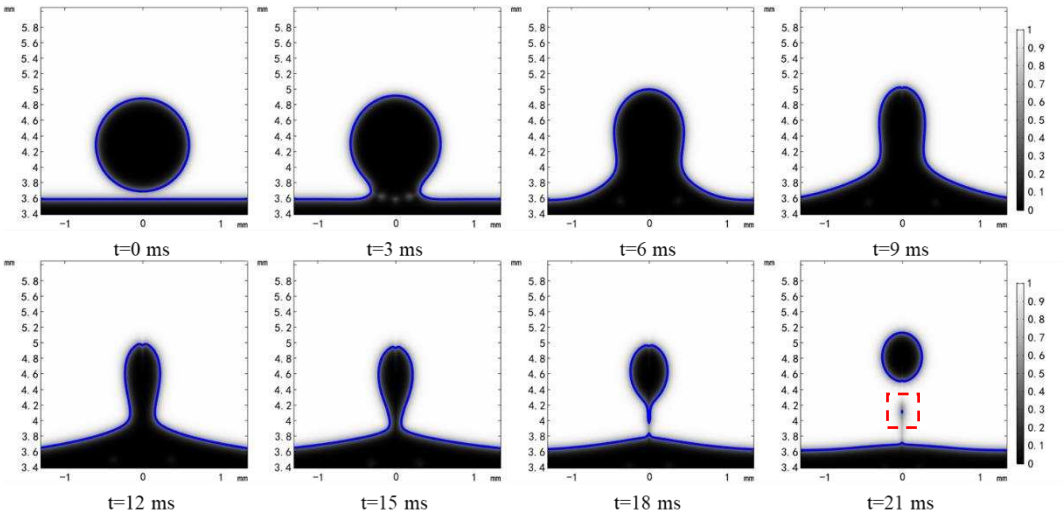

(a)

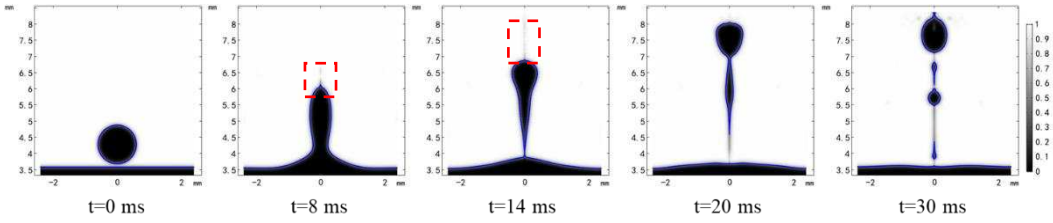

(b)

Fig. 4 Time evolution of the drop-interface partial coalescence: (a) Typical partial coalescence: E=373 V mm^{-1}, D=1.196 mm; σ_w=5.49×10^{-5} S m^{-1}; γ=0.025 N m^{-1}, d=0.1 mm; (b) Jet-like partial coalescence: E=373 V mm^{-1}, D=1.196 mm; σ_w=5.49×10^{-4} S m^{-1}; γ=0.025 N m^{-1}, d=0.1 mm. The fluids properties are given in Table 2.

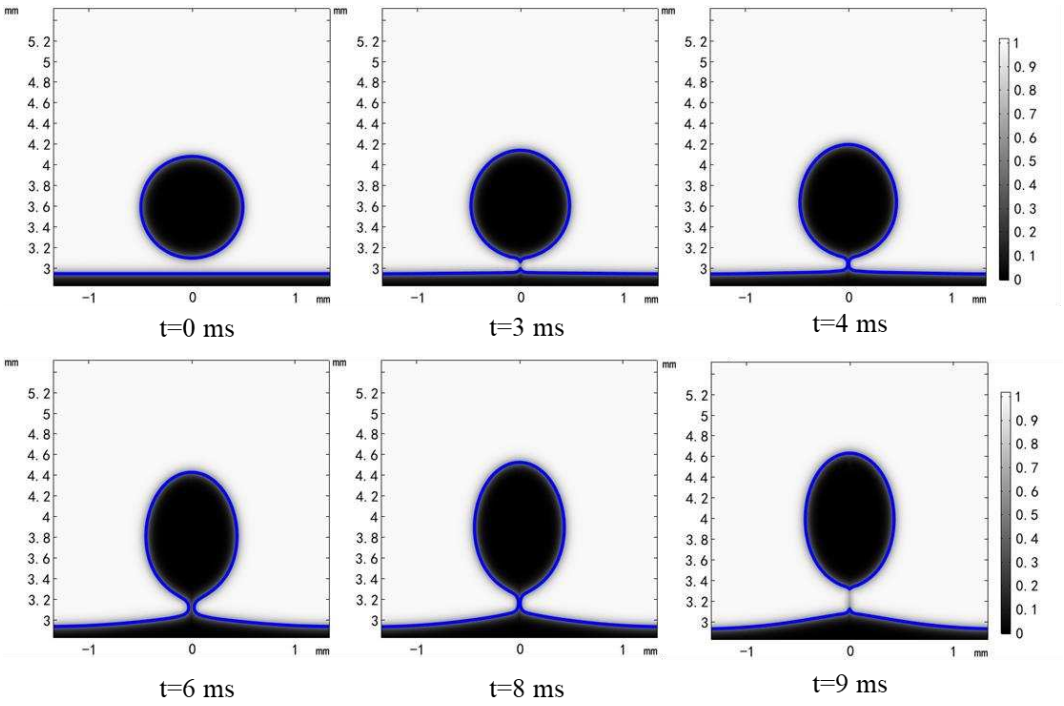

(a)

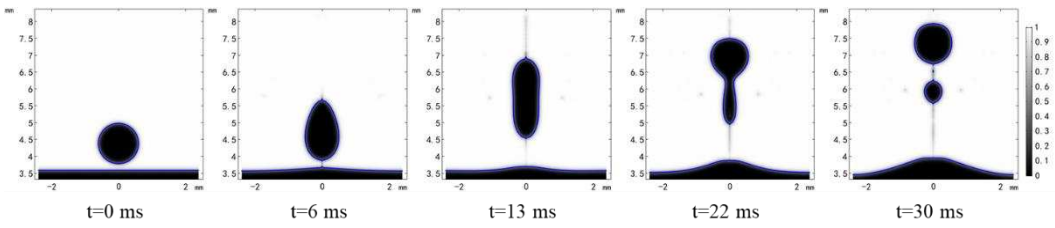

(b)

Fig. 5 Time evolution of the drop-interface non-coalescence: (a) Typical non-coalescence: E=373 V mm^{-1}, D=0.984 mm; σ_w=5.49×10^{-3} S m^{-1}; γ=0.025 N m^{-1}, d=0.15 mm; (b) Breakup of bouncing-off droplet non-coalescence: E=373 V mm^{-1}, D=1.196 mm; σ_w=5.49×10^{-5} S m^{-1}; γ=0.025 N m^{-1}, d=0.2 mm. The fluids properties are given in Table 2.

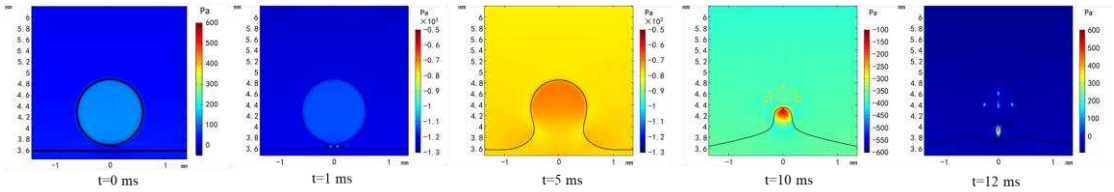

(a)

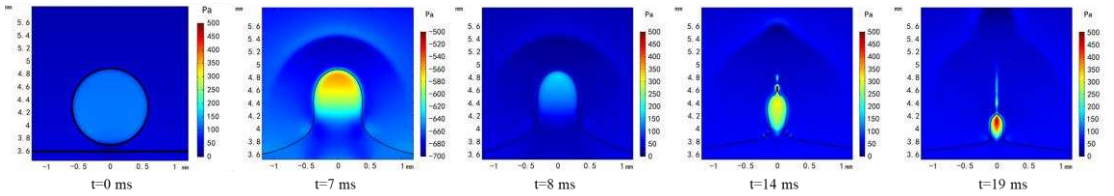

(b)

Fig. 6 Evolution of the pressure field distribution in the complete coalescence mode: (a) Typical complete coalescence: E=373 V mm^{-1}, D=1.196 mm; σ_w=5.49×10^{-5} S m^{-1}; ε_o=1; γ=0.025 N m^{-1}, d=0.1 mm; (b) Complete coalescence with upheaval: E=373 V mm^{-1}, D=1.196 mm; σ_w=5.49×10^{-3} S m^{-1}; ε_o=3; γ=0.025 N m^{-1}, d=0.1 mm. The fluids properties are given in Table 2.

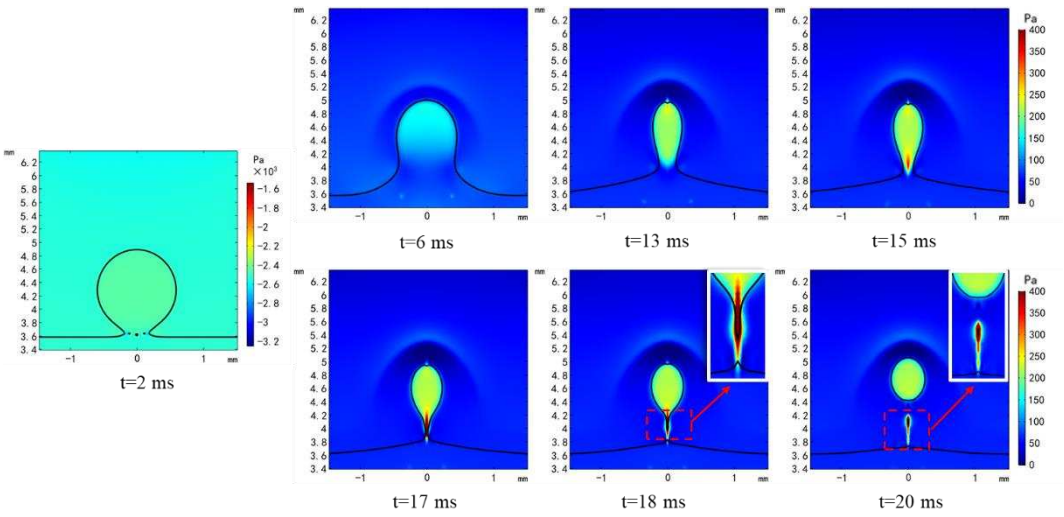

Fig. 7 Evolution of the pressure field distribution in the typical partial coalescence mode. The calculation conditions were: E=373 V mm^{-1}, D=1.196 mm; σ_w=5.49×10^{-5} S m^{-1}; γ=0.025 N m^{-1}, d=0.1 mm and fluids properties are given in Table 2.

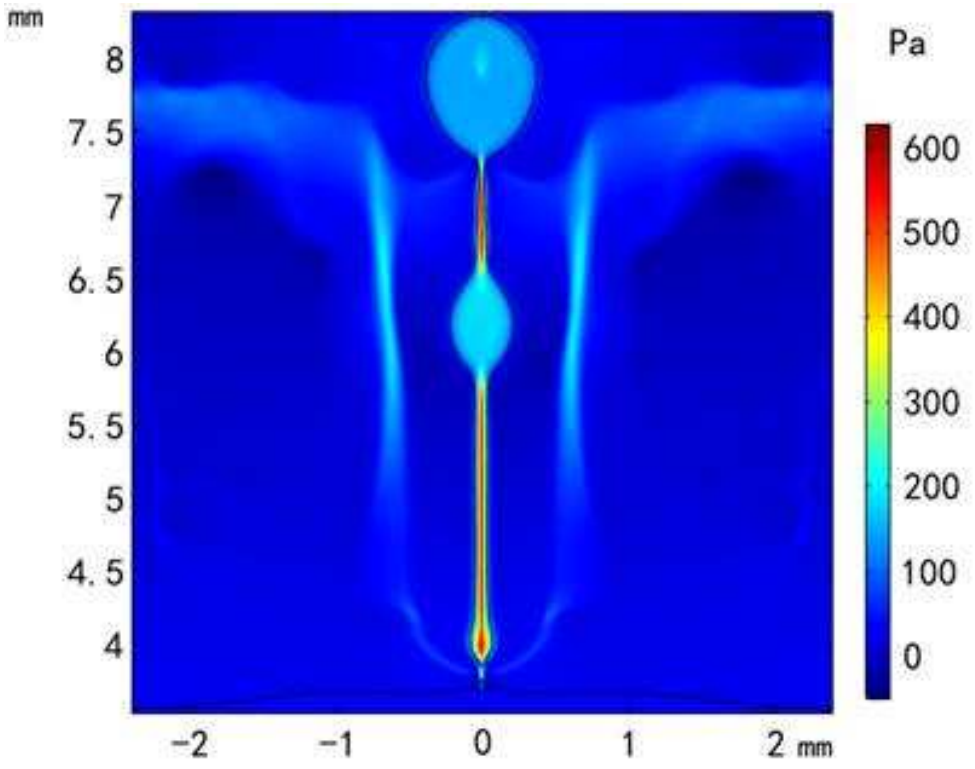

Fig. 8 The pressure field distribution at t=26 ms in the Jet-like partial coalescence mode. The calculation conditions were: E=373 V mm^{-1}, D=1.196 mm; σ_w=5.49×10^{-4} S m^{-1}; γ=0.025 N m^{-1}, d=0.1 mm and fluids properties are given in Table 2.

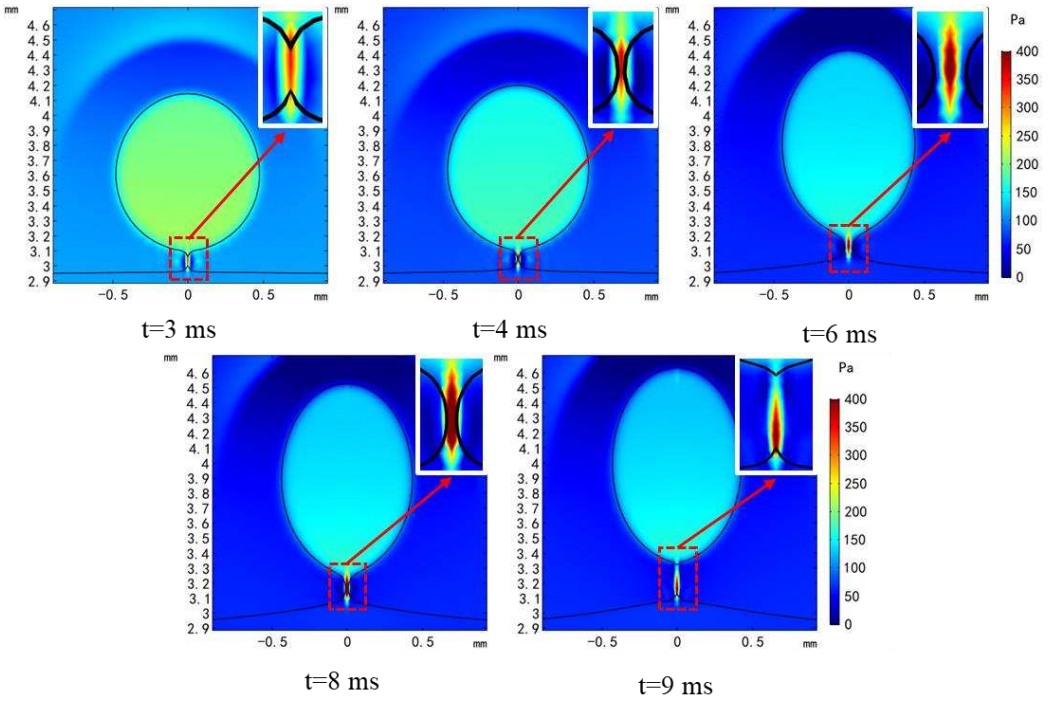

(a)

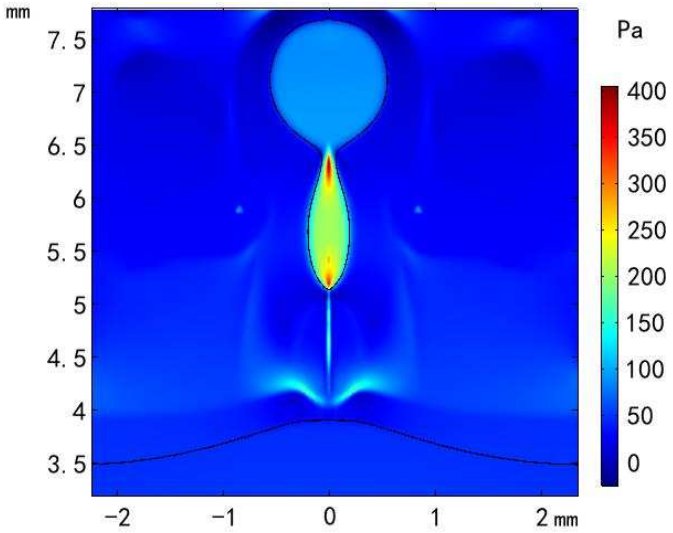

(b)

Fig. 9 Evolution of the pressure field distribution in the non-coalescence mode. (a) Typical non-coalescence: E=373 V mm^{-1}, D=0.984 mm; σ_w=5.49 × 10^{-3} S m^{-1}; γ=0.025 N m^{-1}, d=0.15 mm; (b) Breakup of bouncing-off droplet, t=25 ms: E=373 V mm^{-1}, D=1.196 mm; σ_w=5.49×10^{-5} S m^{-1}; γ=0.025 N m^{-1}, d=0.2 mm. The fluids properties are given in Table 2.

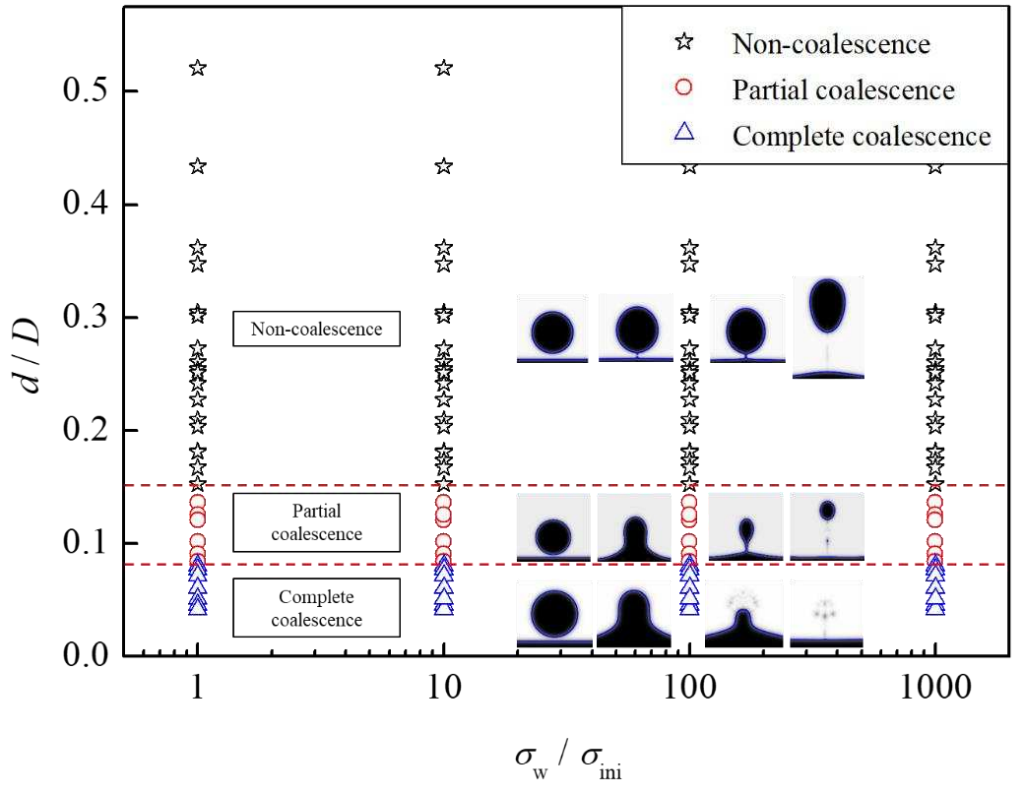

Fig. 10 Simulations are shown for a range of non-dimensional drop-interface distances and non-dimensional water phase conductivity. The red dashed lines are shown to highlight the critical non-dimensional distance.

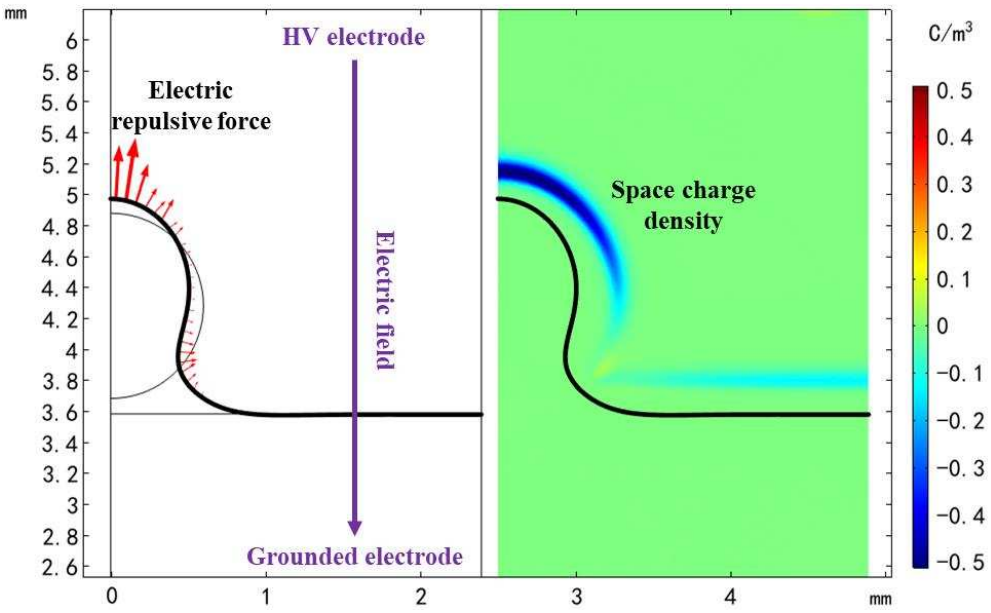

Fig. 11 Electrostatic force and space charge density (C m^{-3}) in the coalescence region after 5 ms. The calculation conditions were: σ_w=5.49×10^{-6} S m^{-1}, *E*=373 V mm^{-1}, *D*=1.196 mm, *d*=0.1 mm. The fluids properties are given in Table 2.

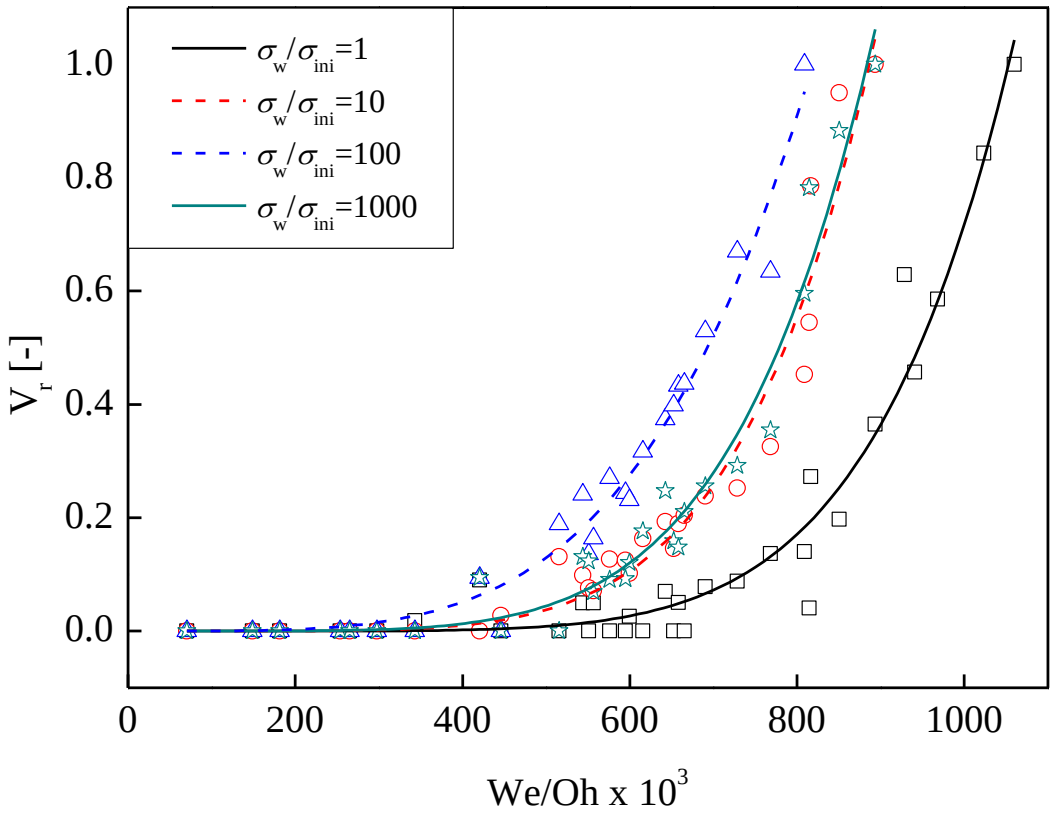

Fig. 12 Calculated volume of the secondary droplet as a function of the We/Oh number. The data points were calculated values for conductivity of σ_w/σ_{ini}=1 (□), σ_w/σ_{ini}=10 (○), σ_w/σ_{ini}=100 (△), and σ_w/σ_{ini}=1000 (☆). The lines are fitted trend lines.